Supporting information

The nanocapsules with dual-targeting of cell and mitochondrial function for enhanced hypoxia-activated drug therapy

Fen Li, Ziyi Li, Jing Zhao, Qingqing Zhang, Mengting Wu, Yingshu Guo*

School of Chemistry and Chemical Engineering, Qilu University of Technology (Shandong Academy of Sciences), Jinan 250353, China.

E-mail: yingshug@126.com

1. Materials and Equipments

1.1. Materials and reagents

Ammonium metavanadate (NH_4VO_3), tirapazamine (TPZ, ≥98%), cytochrome c from pig heart (≥95%), 1,2-dihexadecanoyl-sn-glycero-3-phosphocholine (DPPC), Cerium(III) nitrate hexahydrate ($Ce(NO_3)_3$•$6H_2O$), terephthalic acid (TPA), sodium dithionite ($Na_2S_2O_4$), dimethyl sulfoxide (DMSO), horseradish peroxidase (HRP), 1,2-dioleoyl-sn-glycero-3-phosphate (DOPA), methanol, skim milk, cholesterol, 1,2-Dioleoyl-3-trimethylammonium-propane chloride (DOTAP) were purchased from Macklin Inc.. PBS (pH 7.4,10 mM) and the MUC1 aptamer (5'-cholesterol-GCAGTTGATCCTTTGGATACCCTGG-3') were acquired from Sangon Biotech (Shanghai) Co., Ltd.. 1,2-distearoyl-sn-glycero-3-phosphoethanolamine-N- (methoxy(poly (ethylene glycol))2000) (DSPE-PEG_{2000}), 1,2-distearoyl-sn-glycero-3-phosphoethanolamine -N-(polyethylene glycol)-Triphenyl phosphate (sodium salt) (DSPE-PEG_{2000}-TPP) were purchased from Guangzhou Weihua Biotechnology Co., Ltd.. 2,7-dichlorofluorescein diacetate (DCFH-DA), SOD assay kit, Amplex red, Calcein/PI cell viability/cytotoxicity assay kit, methyl thiazolyl tetrazolium (MTT), DAPI, 2-(4-iodophenyl)-3-(4-nitrophenyl)-5-(2,4-disulfophenyl)-2H-tetrazolium (WST-1) and DiD were purchased from Beyotime Biotechnology. Antibiotics (penicillin-streptomycin, PS), Dulbeccos modified eagles medium (DMEM), trypsin (0.25% EDTA), cell lysis buffer for Western and IP without inhibitors, TBST (20x), stripping buffer, PMSF, BCA protein assay kit, anti-HiF1α polyclonal antibody, anti-β-actin monoclonal antibody were purchased from Beijing Solarbio Science & Technology Co., Ltd.. Ethanol and hydrogen peroxide (H_2O_2, 30%) were obtained from Sinopharm Chemical Reagent Co., Ltd.. Color PAGE Gel Rapid Preparation Kit and PVDF (0.45 μm) were purchased from Epizyme Biotech. Hypersensitive ECL chemiluminescence kit, tris-glycine SDS-PAGE running buffer, tris-glycine transfer buffer were provided from Wuhan Servicebio Technology Co., Ltd.. Fetal bovine serum (FBS) was provided from Biological Industries. MRC-5 cell lines (human embryonic lung fibroblast) and MCF-7 cell lines (human breast cancer) were provided by Procell Life Technology (Wuhan, China). All chemical reagents were used directly without further purification.

1.2. Equipments

The morphology of the nanoparticles was photographed using transmission electron microscopy (TEM, JEOL JEM2100). Scanning electron microscopy (SEM) images were obtained from a Hitachi Regulus8220 scanning electron microscopy. Ultraviolet–visible absorption spectra (UV/vis) were measured by an Agilent Cary 60 UV-vis Spectrophotometer. X-ray photoelectron spectroscopy (XPS) was performed on a Thermo Scientific™ ESCALAB™ Xi+ to determine the valence states of the Ce/V component of $CeVO_4$. X-ray powder diffraction (XRD) patterns was characterized by Rigaku SmartLab SE diffractometer. The Hitachi FL-4700 was used to detect and record the fluorescence signals. The Fourier transform infrared (FT-IR) spectrum was detected by Bruker TENSOR27 FTIR spectrophotometer. Electron paramagnetic resonance (EPR) spectra were acquired on Bruker A300 spectrometer to measure the •OH production capabilities. The

Nikon Ti2-E microscope was utilized to acquire the fluorescence images. Mitochondrial morphology was evaluated by High Content Imaging System (PerkinElmer Opera Phenix). Flow cytometry measurements were performed on Beckman Coulter, CytoFLEX. The protein expression level was monitored by nucleic acid gel imaging analysis system (FluorChem HD2). The mice were photographed using a PerkinElmer IVIS Lumina III imaging system.

2 Experimental procedures

2.1 Synthesis of $CeVO_4$ Nanoparticle ($CeVO_4$ NPs)

To synthesize $CeVO_4$ using the solvothermal method, $Ce(NO_3)_3$•$6H_2O$ solution (10 mL, 1 mM) was subjected to ultrasonic treatment for 10 min, resulting in a slightly transparent mixture. Further, under vigorous stirring, NH_4VO_3 solution (40 mL, 1 mM) was added dropwise to the $Ce(NO_3)_3$•$6H_2O$ solution, maintaining a constant temperature at 25°C. At 90°C, the stirring was kept up for a further 2 hours. The product was then collected via centrifugation. Finally, an oven set to 80°C was used to dry the products.

2.2 Synthesis of $CeVO_4$/TPZ (CZ NC)

Firstly, DOPA in chloroform (0.1 mg, 1 mg/mL) was added into the 2 mL ethanol containing 1 mg $CeVO_4$ nanoparticles 20 min of ultrasonication. After centrifuging the combination solution and washing it with ethanol to get rid of any free DOPA that was not bound, it was once again dispersed in chloroform. Next, containing DOTAP, DPPC, cholesterol, DSPE-PEG_{2000} at a molar ratio of 1:1:1:0.1 (The total amount of liposomes was 10 mg) chloroform solutions were added to the $CeVO_4$-DOPA chloroform solution to perform PEGylation under vigorously stirring overnight. Afterwards, a lipid film was formed by rotary evaporation at 37°C to eliminate the solvent. Next, the flask was then filled with 2 mL of TPZ solution (1 mg/mL) and it was sonicated for 10 min in an ice-water bath.

2.3 Synthesis of $CeVO_4$/TPZ/Apt (CZA NC)

After dispersing the previously synthesized CZ (10 mL) in Apt aqueous solution (2 OD), it underwent a one-minute ultrasonography treatment. For a full day in the dark, the solution was slowly stirred.[1] After that, the unbound Apt was removed from the CZA NC by centrifuging and repeatedly washing. Finally, CZA NC was dispersed in the PBS solution.

2.4 Synthesis of $CeVO_4$/TPZ/TPP (CZP NC)

Following the same procedure mentioned above. Firstly, DOPA in chloroform (0.1 mg, 1 mg/mL) was added into the 2 mL ethanol containing 1 mg $CeVO_4$ nanoparticles 20 min of ultrasonication. After centrifuging the combination solution and washing it with ethanol to get rid of any free DOPA that was not bound, it was once again dispersed in chloroform. Next, containing DOTAP, DPPC, cholesterol, DSPE-PEG_{2000}-TPP at a molar ratio of 1:1:1:0.1(The total amount of liposomes was 10 mg) chloroform solutions were added to the $CeVO_4$-DOPA chloroform solution to perform PEGylation under vigorously stirring overnight. Afterwards, a lipid film was formed by rotary evaporation at 37°C to eliminate the solvent. Next, the flask was then filled with 2 mL of TPZ solution (1 mg/mL) and it was sonicated for 10 min in an ice-water bath.

2.5 Synthesis of $CeVO_4$/TPZ/TPP /Apt (CZPA NC)

After dispersing the previously synthesized CZP (10 mL) in Apt aqueous solution (2 OD), it underwent a one-minute ultrasonography treatment. For a full day in the dark, the solution was slowly stirred.[1] After that, the unbound Apt was removed from the CZPA NC by centrifuging and repeatedly washing. Finally, CZPA NC was dispersed in the PBS solution.

2.6 Determination of Cyt c Oxidase-like Activity of $CeVO_4$ NPs

The ferrous Cytochrome c (Cyt c) was prepared by adding $Na_2S_2O_4$ to the solution of ferric cytochrome c from pig heart.[2] The enzyme purification was conducted using a Sephadex G-25 PD-10 desalting column that had been equilibrated with PBS to remove excess $Na_2S_2O_4$.

Cyt c absorbance at 550 nm was measured with an ultraviolet/visible spectrophotometer. The reaction mixture contained CeVO4 NP (30 μg/mL) and Cyt c (10 μM /mL) in PBS.

2.7 Determination of Partially Reduced Oxygen Species (PROS) Generation in Solution

The product of the cytochrome c oxidase (CcO)-like reaction was determined using a variety of assays. Firstly, WST-1 was utilized for determining the production of superoxide during the reaction.[3] The WST-1 combines with superoxide to combines spectrophotometrically detectable formazan, with an maxima absorption at 440 nm. The reaction solution contained WST-1, nanozymes (25 ng/μL) and Cyt c (10 μM/mL) in PBS in the presence of WST-1 and the absorbance was determined at 440 nm.

Further, to eliminate the possible production of H_2O_2, Amplex red assay was used.[4-6] In brief, Amplex red is oxidized by HRP in presence of H_2O_2 to a fluorescent product (resorufin) having an excitation maximum at 563 nm and emission maximum at 587 nm. Therefore, the production of H_2O_2 during the reaction between $CeVO_4$ NP and Cyt c can be monitored by Amplex Red-HRP-coupled assay. The reaction mixture contained $CeVO_4$ NP (25 ng/μL), Cyt c (10 μM/mL), HRP (0.5 mg/mL), Amplex red (10 μM) in PBS.

To rule out the probable production of •OH during the reaction, the highly luminous 2-hydroxy terephthalic acid is formed when TPA interacts with •OH having 315 nm excitation and 425 nm emission.[7] The 1 mL reaction solution contained $CeVO_4$ NP (25 ng/μL), Cyt c (10 μM/mL), TPA (1 mM) in PBS. The positive control contained H_2O_2 (10 mM), $CuSO_4 \cdot 5H_2O$ (20 μM) and TPA (1 mM) in PBS.

EPR was further used to determine the ability to generate •OH. The reaction was performed by mixing ferrous Cyt c (0.5 mL, 0.2 mM) with $CeVO_4$ suspension (0.1 mL 1 mg/mL). The spectrum was collected after mixing and reacted for 1 h. Control experiment was performed with 0.2 mM Fe^{2+} solution by addition of 0.2 mM H_2O_2 and DMPO (100 mM), and the spectrum was collected after mixing under the same conditions.[8]

2.8 Examining CcO-like Catalytic Activities of $CeVO_4$ NPs

The reaction mixture contained CZPA NC (30 μg/mL) and Cyt c (10 μM/mL) in PBS. Meanwhile, a portable dissolved oxygen meter was used to track the amount of oxygen consumed. Free CZPA, Cyt c, and "CZPA + Cyt c" combined reaction systems were measured for

comparison.

2.9 Drug Loading Efficiency and Encapsulation Efficiency.

The payload of TPZ was obtained by using the standard calibration curve based on the difference of the UV-vis absorption intensity at 470 nm between the supernatant collected after centrifugation and initial solution. The encapsulation efficiency (EE) and the drug loading efficiency (LE) could be calculated according to the following equations.

$$\text{EE\%} = \frac{\text{Weight of drug encapsulated}}{\text{Total weight of drug used}} \times 100\%$$

$$\text{LE\%} = \frac{\text{Weight of drug loaded}}{\text{Weight of drug and nanoparticals}} \times 100\%$$

2.10 Cell Culture

MCF-7 cell lines and MRC-5 cell lines were cultured in DMEM high-glucose medium supplemented with 10% heat-inactivated FBS and 1% PS at 37℃in a humidified atmosphere with 5% CO_2.[9]

2.11 Cytotoxicity Assay

The MTT viability kit was used to quantify the cytotoxicity. Taking the measurement of MCF-7 cells for example, the 96-well plates containing the cells were left to grow for 24 hours. The plates were filled with various nanoparticle concentrations in DMEM media (0, 10, 20, 30, 40 μg/mL). Subsequently, each well received MTT reagent (5 mg/mL), and an extra 4 hours were spent incubating the plate. Each well was filled with DMSO after the supernatant was removed. A microplate reader measured absorbance of each well at 492 nm after 5 min.[10]

2.12 Evaluation of Cellular Apoptosis by Live/dead Assay

Firstly, after being cultivated, the MCF-7 cells were given various treatments. The concentrations of $CeVO_4$, TPZ, CZ, CZP and CZPA were all 30 μg/mL. After 24 hours incubation, the cells were incubated with Calcein-AM (2 μM) and PI (3 μg/mL) for 30 min. In the end, a fluorescent microscope was used to directly photograph these cells. Calcein-AM can stain green, living cells, and PI can stain red, dead cells.[11]

2.13 Aptamer Affinity Analysis

The targeting ability of Apt was investigated using MCF-7 and MRC-5 cells. The DiD-labeled CZPA or CZP NC (30 μg/mL) were added to 12-well plates and incubated for different time intervals 0,1, 2, 3 hours respectively.

2.14 Evaluation of Targeted Mitochondria

MCF-7 cells were cultured and grown with CZP NC, CZPA NC (30 μg/mL) for 8 hours after being cleaned with PBS. After removing from the incubator and giving two PBS washes, the cells were filled with the Mito-Tracker Green fluorescence probe and let to incubate for 0.5 hours. MCF-7 cells were measured using fluorescence microscope. Using the Image J software, the Pearson's correlation coefficients were obtained.[12, 13]

2.15 Determination of Intracellular O_2

A probe for measuring O_2 levels, $[(Ru(dpp)_3)]$ Cl_2 was employed to investigate the consumption

of O_2 by tumor cells.[14] MCF-7 cells were treated with different formulations ($CeVO_4$, TPZ, CZ, CZP and CZPA, 30 μg/mL), RDPP was added to the cells and incubated for 4 hours. Lastly, the [$(Ru(dpp)_3)$] Cl_2 fluorescent signal in the cells was examined and captured on camera using a fluorescent microscope.

2.16 Detection of Intracellular ROS

The production of ROS was measured with the ROS probe DCFH-DA. Specifically, MCF-7 cells after different treatments were collected and loaded with 10 μM DCFH-DA for 15-30 min.[15]

2.17 Detection of Intracellular •OH

Using the HPF probe, intracellular •OH production was found. After MCF-7 cells were cultured 24 hours, the cells were treated with various nanoparticles for 6 hours. After the medium was removed, the cells were incubated with HPF solution (10 μM) for 20 min. Using a flow cytometer and fluorescent microscope, the cells were examined after being cleaned with PBS to eliminate any remaining probe.

2.18 Detection of Mitochondrial Membrane Potential

MCF-7 cells were cultured for 24 hours. A medium solution containing PBS, $CeVO_4$, TPZ, CZ, CZP and CZPA NC (30 μg/mL) was used in place of the original medium. Following an additional 8 hours of culture, JC-1 staining was carried out as directed by the manufacturer and monitored by fluorescence microscope.

2.19 Measurement of Intracellular ATP Content

6-well plates were used to seed the MCF-7 cells, which were cultured for 24 hours. Then, the cells were treated with PBS, $CeVO_4$, TPZ, CZ, CZP and CZPA NC (30 μg/mL) respectively. An additional 4 hours were spent incubating the cells and cleaned with PBS. Then, they were treated in accordance with the ATP assay kit's protocol.[16]

2.20 Western Blot Analysis

In order to examine the expression of the protein, MCF-7 cells were plated on a 6-well plate, and after 12 hours, PBS, $CeVO_4$, TPZ, CZ, CZP, and CZPA NC (30 μg/mL) were added to the plate, after culturing for 6 hours, protein expression in cells was analyzed by the western blot method. After centrifugation (12000 rpm,10 min), the supernatants were collected. The BCA method was used to measure the protein contents in supernatants. Following their separation via 10% sodium dodecyl sulfate polyacrylamide gel electrophoresis, the samples were moved onto polyvinylidene difluoride membranes. Membranes were stained overnight at 4°C with rabbit anti-HIF1α antibody after being blocked for 1 hour with skimmed milk in TBST and anti-β-actin antibody as the loading control. HRP-labeled secondary antibodies were added to the membranes and incubated for 1 hour after three rounds of TBST washing. The bands were detected using a hypersensitive ECL chemiluminescence kit and imaged by western blotting and nucleic acid gel imaging analysis system.

2.21 Animal Model

BALB/c nude mice were purchased from Beijing Vital River Laboratory Animal Technology

Co., Ltd. This work has received approval for research ethics from Science and Technology Ethics Committee, Linyi People's Hospital (202311-A-005). MCF-7 cells were used to establish the tumor-bearing mice model. Once the tumor volume reached approximately 100 mm^3, the tail vein was injected with DiD-labeled CZPA NC (10 mg kg^{-1}). Then, the mice were anesthetized using isoflurane and photographed using a PerkinElmer IVIS Lumina III imaging system at 2, 4, 8, 12 and 24 hours post-injection. After 14 days, the mice were killed, the primary organs (heart, liver, spleen, lung, and kidney) were taken out for histological and imaging, and the tumor only for imaging.

2.22 Hemolysis Assay

Fresh blood from BALB/c nude mice was centrifuged at 4℃. The precipitate was then washed three times with PBS. Subsequently, 20 μL of erythrocytes was resuspended in 480 μL of saline, resulting in a 4% (v/v) cell suspension. 500 μL of CZPA NC at various concentrations was added to the cell suspension in order to measure hemolysis, and the hemolysis was observed after mixing. The mixture was incubated for 3 hours, then centrifuged at 4℃. The absorbance of the supernatant was determined at 540 nm using a spectrophotometer, and the absorbance measurements were used to compute the hemolysis rate.

Statistical Analysis: The data-related significant difference was calculated utilizing one-way analysis of variance. The probability (p) was statistically significant difference during *$p < 0.05$, **$p < 0.01$, ***$p < 0.001$, and ****$p < 0.0001$.

3 Intermolecular interactions involved in the preparation of CZPA NC

First, DOPA was conjugated on the surface of $CeVO_4$ nanoparticles through phosphate groups in DOPA and Ce ions in nanoparticles to form hydrophobic surface. Then, DPPC, cholesterol, DSPE-PEG_{2000}-TPP and DOTAP were successively added to the chloroform solution, dissolved and then added to $CeVO_4$-DOPA to form $CeVO_4$-PEG through hydrophobic interaction.[17,18] The reason that TPZ molecules can be integrated into $CeVO_4$ nanoparticles was the encapsulation of the hydrophobic drug TPZ through hydrophobic and hydrophobic interactions.[19] Among them, DSPE-PEG_{2000}-TPP has long cycling and mitochondrial targeting properties.[20-22] DOTAP was a positively charged lipid, which give the $CeVO_4$-PEG lipid membrane a positive charge.[23] Since the MUC1 aptamer was negatively charged and the MUC1 aptamer was modified with a cholesterol at 5' end, it can be bound to CZP by electrostatic adsorption and intercalation of cholesterol into the lipid layer to form CZPA NC.[24]

4 The difference between CZ and CZP

Since Cyt c is localized to mitochondria and facilitates electron transport in the cellular respiratory chain, almost 90% of the respiratory oxygen in mammalian cells is consumed by cytochrome c oxidase. The protein Cyt c provides electrons to CcO, which catalyzes the four-electron reduction of oxygen to water. We have carefully discussed the difference between CZ NC and CZP NC. CZ NC had no mitochondrial targeting ligand, and it had a small chance of entering the mitochondria. CZP NC was that once internalized by tumor cells, the TPP mitochondrial targeting ligand in CZP NC helped them localize at mitochondria. The CZP NC would generate ROS to cause mitochondrial dysfunction and lead to cell death efficiently.

5 *In vivo* tumor therapy studies

In the *in vivo* efficacy testing, we provided additional controls to support the effect of CZPA NC on tumor growth. In Fig. 3c, the tumor growth speed of the $CeVO_4$ and TPZ treated group were similar to PBS group, suggesting that $CeVO_4$ and TPZ had no inhibition effect on tumor. It was found that CZ-treated tumor was inhibited to some extent, the reason was that $CeVO_4$ exaggerated the hypoxia condition. TPZ can be triggered sufficiently to further produce BTZ and •OH under hypoxic conditions, which induced DNA damage. Furthermore, CZP exhibited better tumor inhibition effect than CZ, by impairing the mitochondrial membrane potential and decreasing ATP production. Of particular note, CZPA group achieved the most effective tumor growth inhibition, due to dual-targeting and activated TPZ caused by $CeVO_4$-aggravated hypoxia.

In Fig. S24-Fig. S26, we can see that the killing effect of harmful oxidative free radicals on tumor cells was consistent with the trend of tumor growth. In Fig. S24, the control cells and those treated with $CeVO_4$, weak DCF fluorescence was observed. Additionally, there was little fluorescence in the TPZ-treated cells because the hypoxia-activatable drug was not harmful in the nonhypoxic environment. Compared to the controls, the increased fluorescence signals in the cells treated with CZ, CZP, or CZPA could potentially be linked to the rise in ROS production. This increase in ROS was likely a result of oxygen consumption facilitated by the $CeVO_4$-induced CcO-like reaction, as well as the ROS generated by TPZ in response to these changes. In Fig. S25 and Fig. S26, the specific fluorescent probes were used to detect •OH. Compared with PBS group, $CeVO_4$ group and TPZ group, the fluorescence intensity and flow cytometric analysis of CZ group was significantly enhanced due to TPZ can be activated with $CeVO_4$ to produce OH. Moreover, the CZPA group showed further enhanced fluorescence as a result of the increase in internalization mediated by the Apt, which indicated intracellular •OH concentration increasing. By observing the changes in tumor volume after treatment with different nanoparticles (Fig. 3c), the trend was found to be consistent with that at the cellular level. These results indicated that tumor growth inhibition was caused by harmful oxidizing free radicals.

5 Supplementary figures

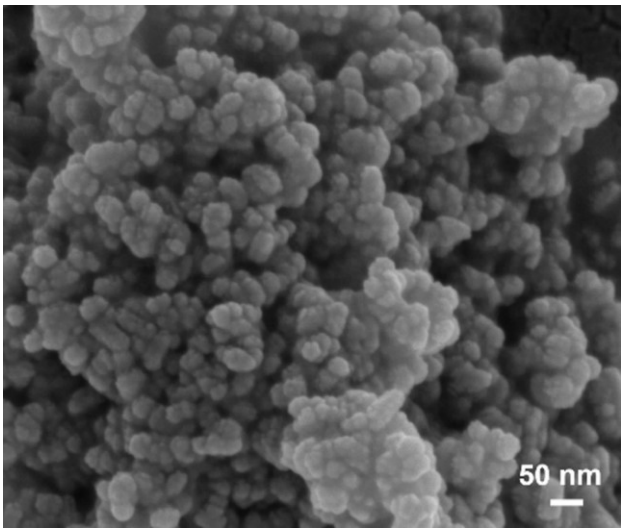

Fig. S1. SEM image of $CeVO_4$ NPs. Scale bar: 50 nm.

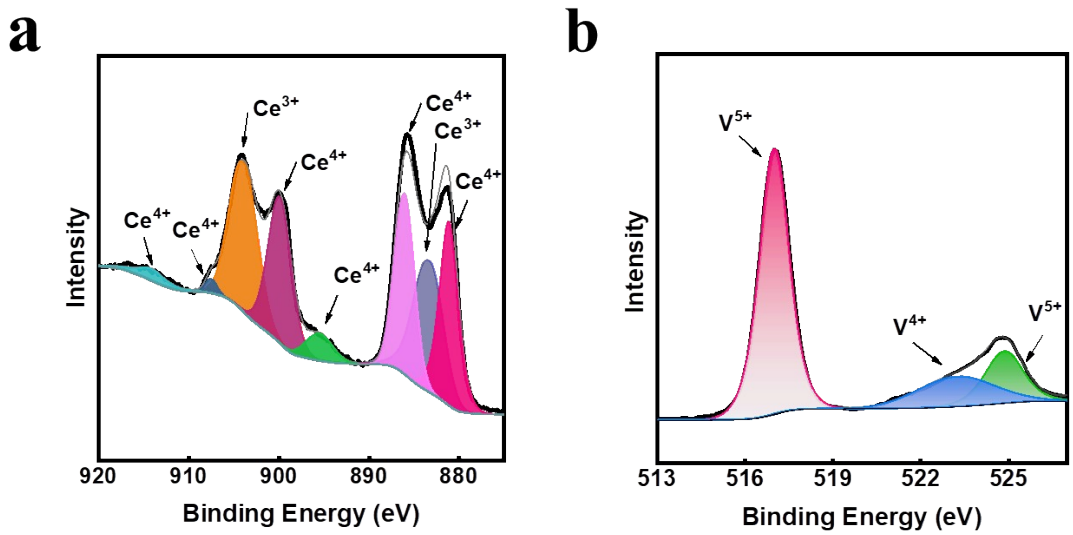

Fig. S2. XPS spectra of Ce 3d (a) and V 2p (b) of $CeVO_4$ NPs. (a) The signal in the Ce 3d XPS can be fitted to Ce^{3+} and Ce^{4+}, indicating that it has a mixed valence feature.[25] the CcO activity can be increased by increasing the number of Ce^{4+} ions on the surface.[26] (b) V^{5+} and V^{4+} were both present in the V 2p XPS.

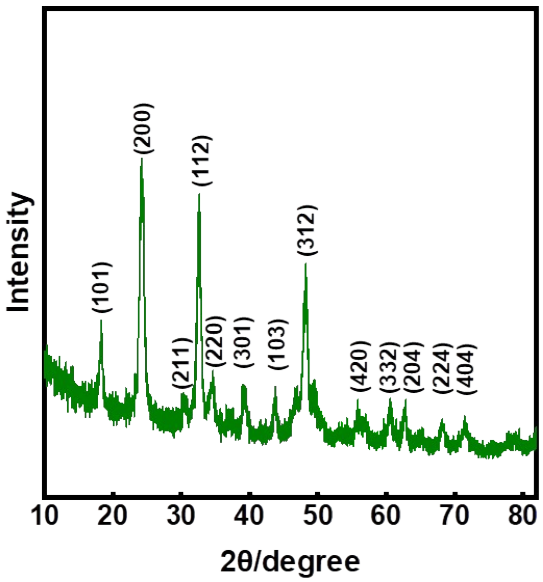

Fig. S3. XRD pattern of $CeVO_4$ NPs. The prepared $CeVO_4$ series of diffraction peaks correspond to the $CeVO_4$ standard card (JCPDS No.12-0757).[27]

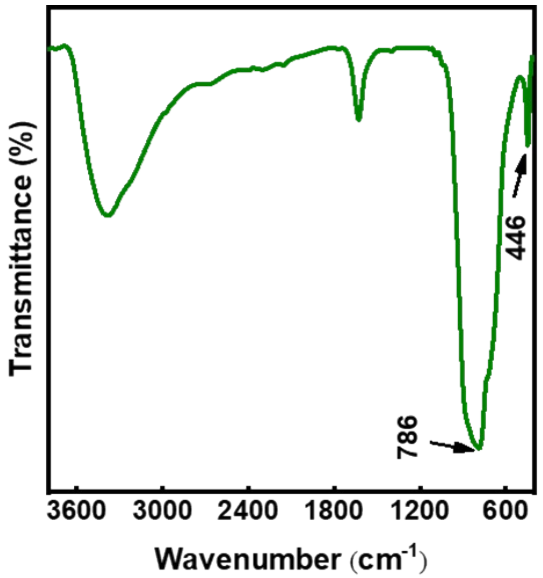

Fig. S4. FT-IR spectra of $CeVO_4$ NPs. The distinct peaks at 445 cm^{-1} and 776 cm^{-1} correspond to the stretching vibration of Ce-O and V-O bonds respectively. The surface of $CeVO_4$ NPs showed shallow bands of O-H stretching and bending at 3400 cm^{-1} and 1600 cm^{-1}, respectively, which corresponded to the absorbed water molecules.[28, 29]

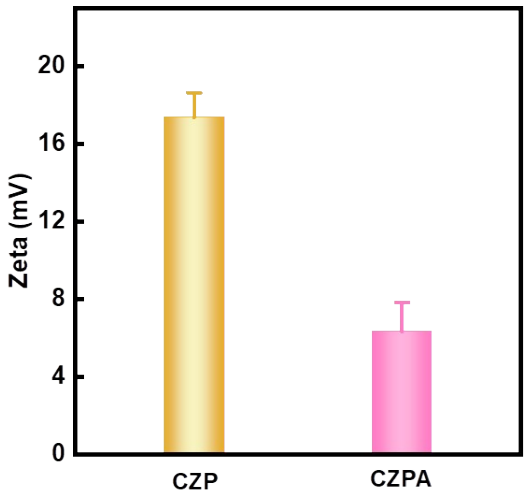

Fig. S5. Zeta potentials of CZP and CZPA. The zeta potential of CZPA was significantly reduced compared to the CZP of +17.3 mV. This was a decrease in positive potential due to the electronegativity of the aptamer.

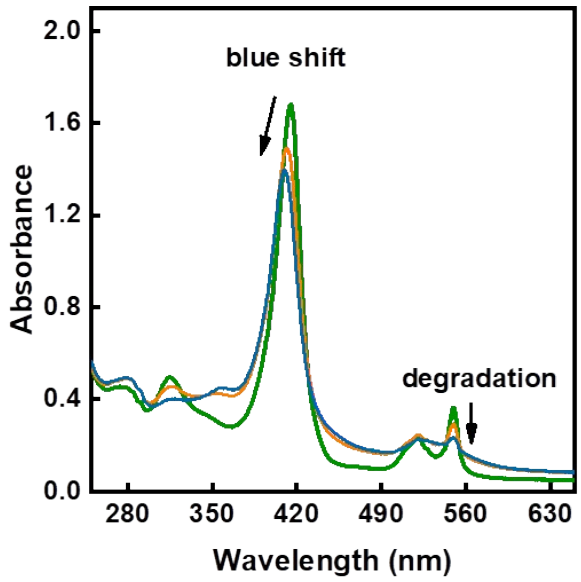

Fig. S6. UV/Vis spectrum alterations of ferrous cytochrome with $CeVO_4$ NPs presence. The absorption peaks at 414 nm and 550 nm were used to identify the ferrous Cyt c.[30, 31] In the presence of $CeVO_4$ NPs, Cyt c was oxidized due to the electron transfer from ferrous to O_2.

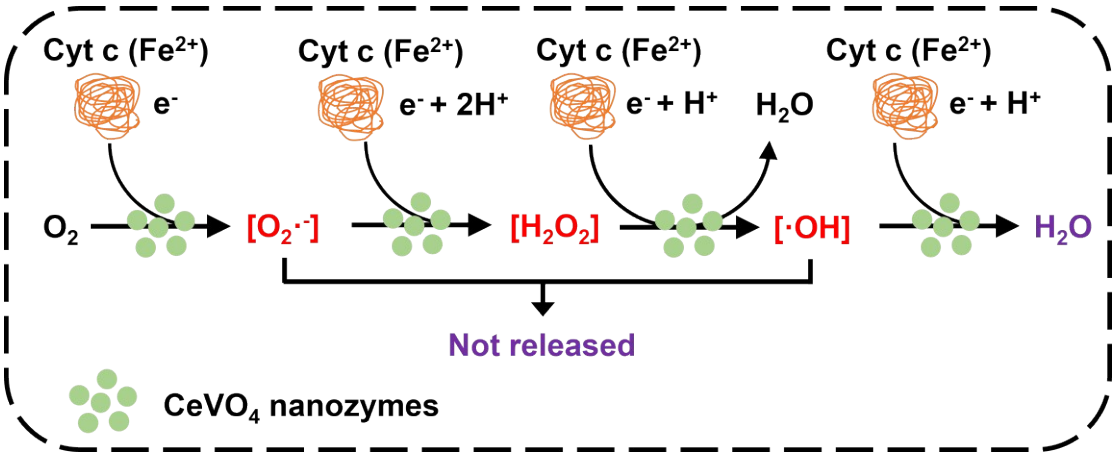

Fig. S7. An illustration showing how O_2 is reduced to water using four electrons, along with the intermediates involved in the reaction.

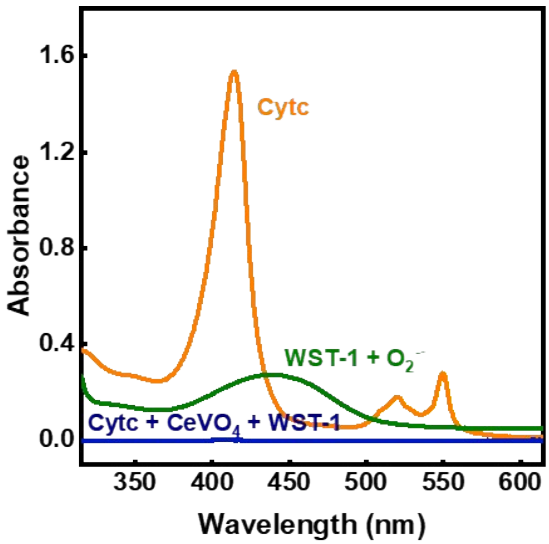

Fig. S8. Determination of $O_2^{\cdot-}$ production using WST-1. The generation of $O_2^{\cdot-}$ through the 1e-reduction of dioxygen was excluded based on an assay using WST-1 dye. In the presence of $O_2^{\cdot-}$, WST-1 dye can react to form a formazan compound, which exhibits a maximum absorption peak at approximately 440 nm. When $CeVO_4$ interacted with Cytc, there was no maximum absorption peak at 440 nm, indicating that no $O_2^{\cdot-}$ is produced.

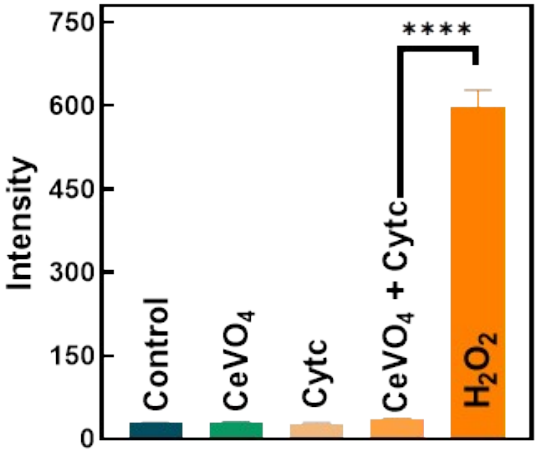

Fig. S9. Measurement of H_2O_2 production using Amplex red. Mean ± SD (n = 3). ****P < 0.0001. Using H_2O_2-specific Amplex Red assay also ruled out the possibility of H_2O_2 release by 2e reduction.[4-6] HRP catalyzed the reaction with Amplex Red in the presence of H_2O_2, producing resorufin. After $CeVO_4$, Cytc and "$CeVO_4$+ Cytc" interacted with HRP and Amplex Red respectively, almost no fluorescence product resorufin was produced, indicating that no H_2O_2 was produced.

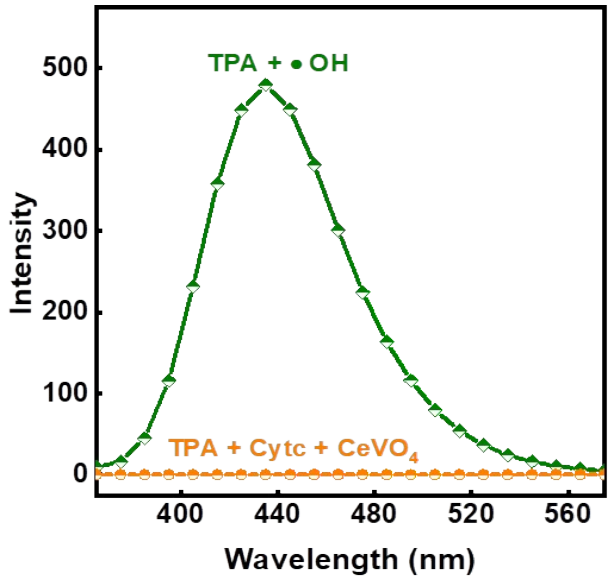

Fig. S10. Determination of ·OH by fluorescence spectroscopy using TPA. The possibility of formation of ·OH was further studied. TPA was used, and the change in fluorescence was measured.[7, 32] Fluorescence increased when TPA reacted with ·OH. The reaction of $CeVO_4$ NPs with Cyt c in the presence of TPA did not show appearance of fluorescent peak confirming the absence of ·OH generation during the reaction.

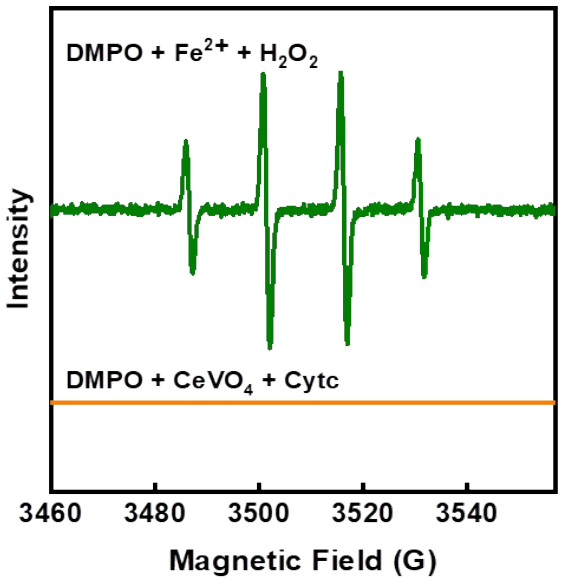

Fig. S11. EPR spectra analysis of the reaction between ferrous Cyt c and $CeVO_4$ suspension. EPR spin-trapping studies further confirmed that no ·OH, were formed.

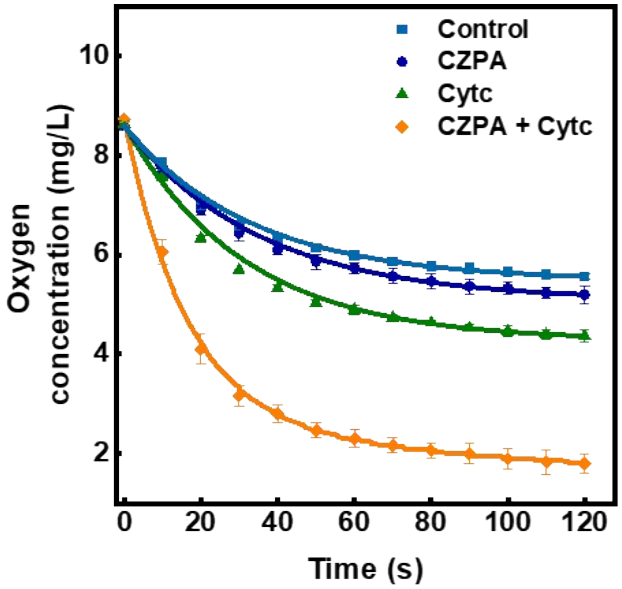

Fig. S12. O_2 consumption by Cyt c, CZPA NC, and "Cyt c + CZPA NC" under atmospheric pressure. With ferrous Cyt c present, CZPA NC significantly depleted O_2, by contrast, without Cyt c, CZPA NC exhibited no catalytic activity.

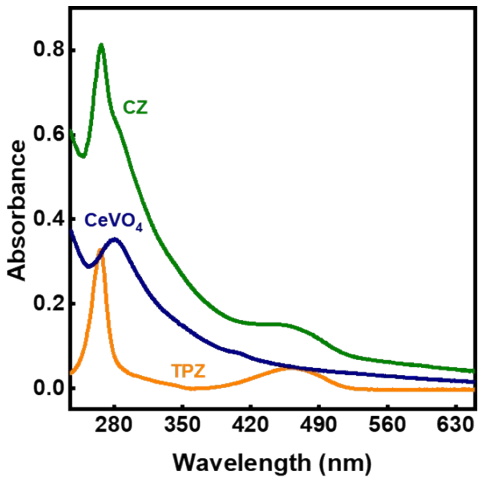

Fig. S13. UV/Vis curves of $CeVO_4$, TPZ, CZ. The UV/Vis absorption spectrum of CZ revealed an apparent TPZ characteristic absorption peak at 470 nm, showing that TPZ had been successfully loaded.[33]

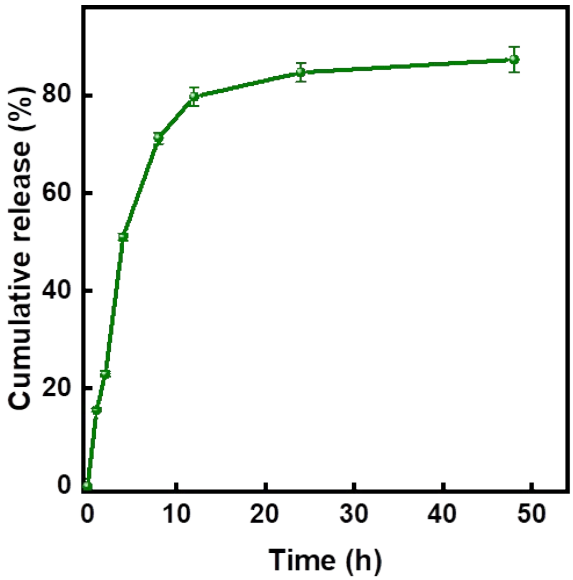

Fig. S14. TPZ release profiles from CZPA.

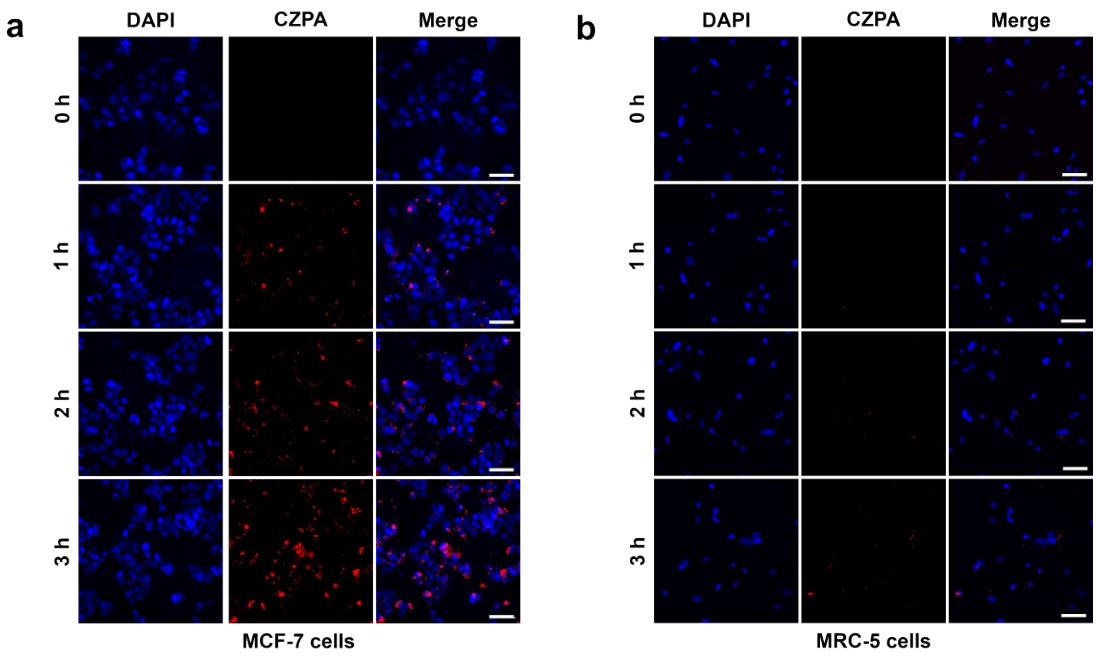

Fig. S15. (a, b) Fluorescence images of CZPA NC in MCF-7 and MRC-5 cells: nuclei stained with DAPI and CZPA NC labeled by DiD. Scale bars: 50 μm.

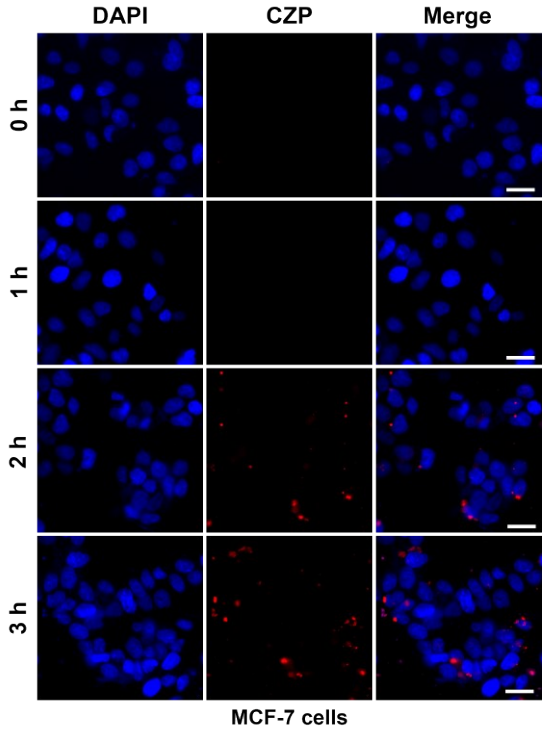

Fig. S16. Fluorescence images of CZP NC in MCF-7 cells: nuclei stained with DAPI and CZP NC labeled by DiD. Scale bars: 20 μm.

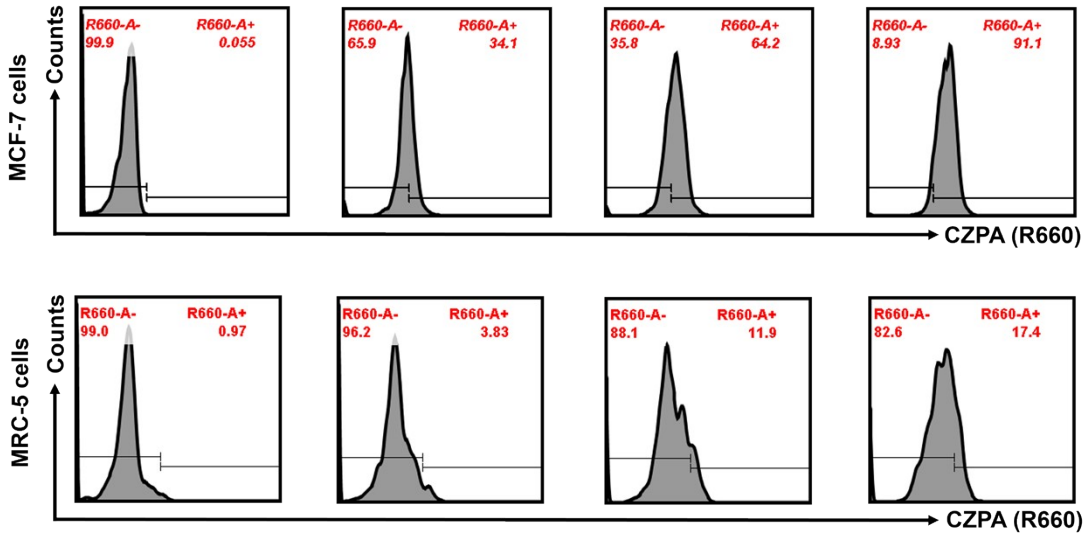

Fig. S17. Flow cytometry analyses of MCF-7 cells and MRC-5 cells incubated with CZPA NC.

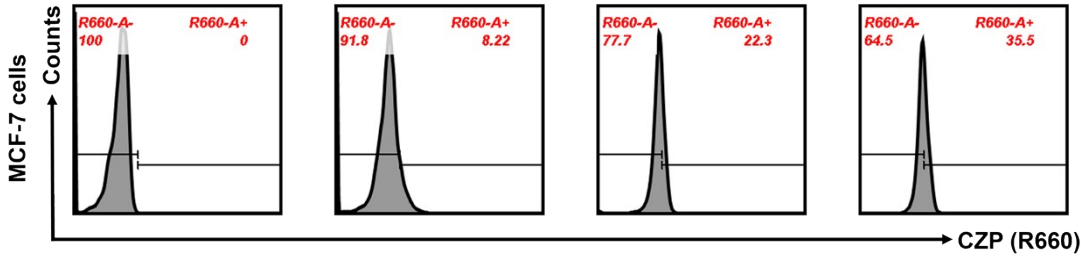

Fig. S18. Flow cytometry analyses of MCF-7 cells incubated with CZP NC.

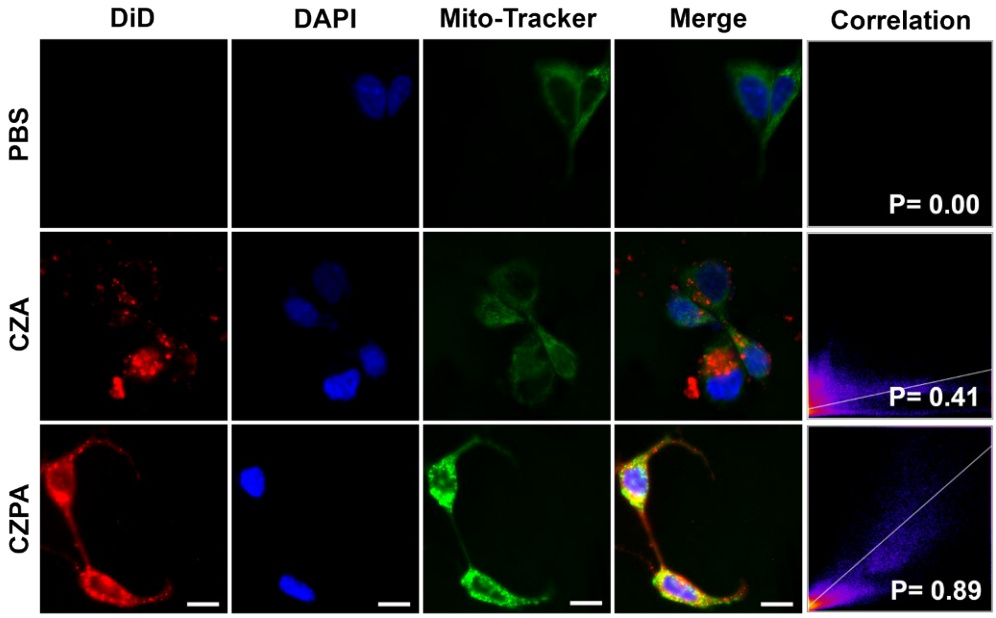

Fig. S19. Subcellular localization between the DiD-labeled CZA NC (or CZPA NC) and Mito-tracker. R is the red and green fluorescence's Pearson correlation coefficient. Scale bar: 10μm.

By gathering wavelengths between 500 and 600 nm, the fluorescence of Mito-Tracker Green was found. The fluorescence of DiD-labeled CZP NC and CZPA NC in the range of 600 ~ 700 nm were collected. Pearson's correlation coefficients of the CZPA group (0.89) was larger than the PBS group (0.0) and the CZP NC group (0.41), which illustrated that once internalized by MCF-7 cells. CZPA NC could localize to mitochondria as a result of an electrostatic contact between its TPP ligand and mitochondria.[14]

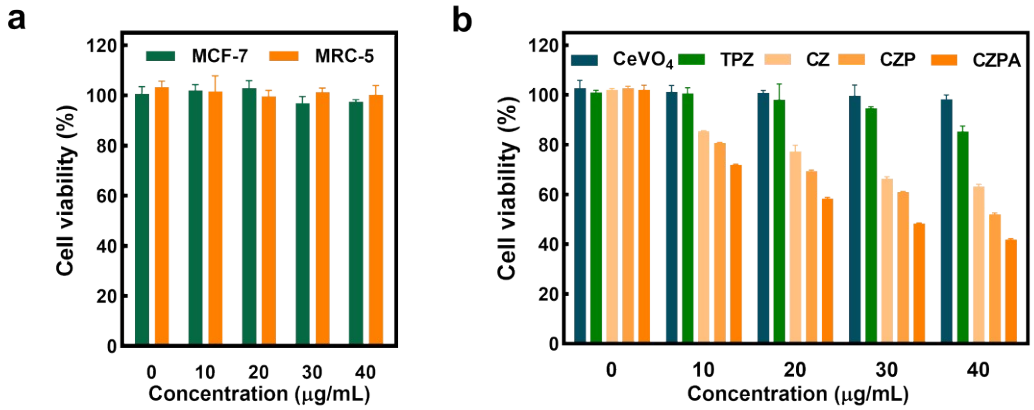

Fig. S20. (a) The survival of MCF-7 and MRC-5 cells following exposure to different $CeVO_4$ concentrations. Mean ± SD (n = 3). (b) Cell viabilities of MCF-7 cells with different treatments. Mean ± SD (n = 3).

The cytotoxic effects of several nanoparticles on MCF-7 cells were also evaluated using the MTT assay. As can be shown in **Fig. S20b**, the MCF-7 cell viability was over 98% at a free TPZ dose of 10 μg/mL, this was owing to the fact that slight hypoxia hindered the activation of the free TPZ, which was consistent with its hypoxia-activated feature. But the cell viability decreased rapidly with the increase concentrations of CZ NC, CZP NC and CZPA NC. When the cells were cultured with CZ NC and CZP NC, the concentration reached 40 μg/mL, resulting in MCF-7 cell viability decreasing to approximately 62% and 50%, respectively. However, MCF-7 cell viability in the CZPA NC treated group reduced to ~41% due to dual-targeting and activated TPZ caused by $CeVO_4$-aggravated hypoxia.

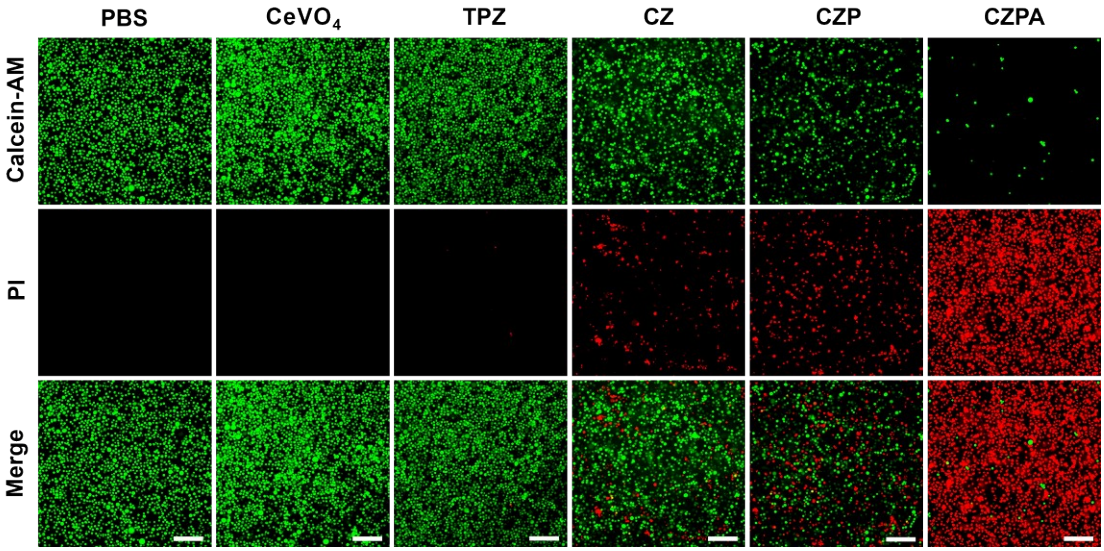

Fig. S21. Calcein-AM/PI staining of MCF-7 cells treated at different conditions. Scale bars: 100 μm. The hypoxic microenvironment was conducive to the activation of TPZ. Following treatment with $CeVO_4$, all MCF-7 cells fluoresced green, suggesting that $CeVO_4$ was highly biocompatible in a physiological setting. When cells were treated in a hypoxic environment, red fluorescence was clearly visible, indicating that CZPA has the responsive activation capability to lead to effective treatment.

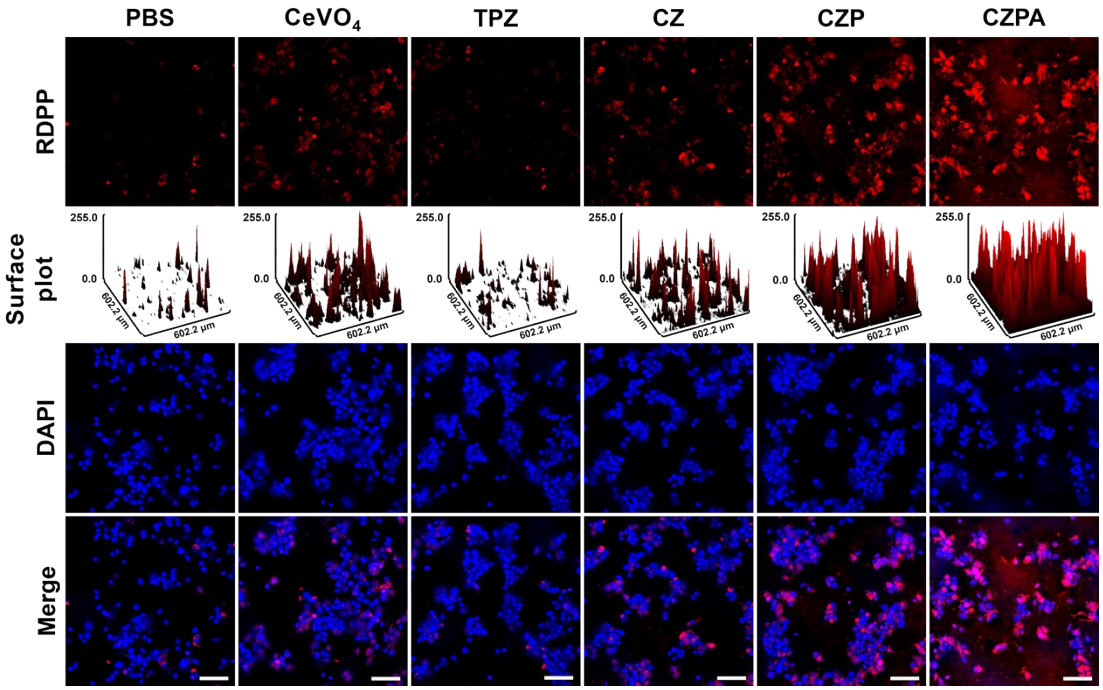

Fig. S22. Fluorescence images for evaluating intracellular oxygen level in MCF-7 cells using O_2 probe ($[Ru(dpp)_3]$ Cl_2, RDPP) with various treatments. Scale bar: 100 μm.

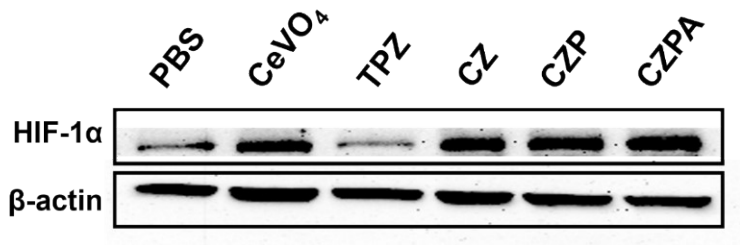

Fig. S23. HIF-1α expression in response to different treatments in MCF-7 cells, as shown by Western blot analysis. β-Actin served as a housekeeping gene for normalization.

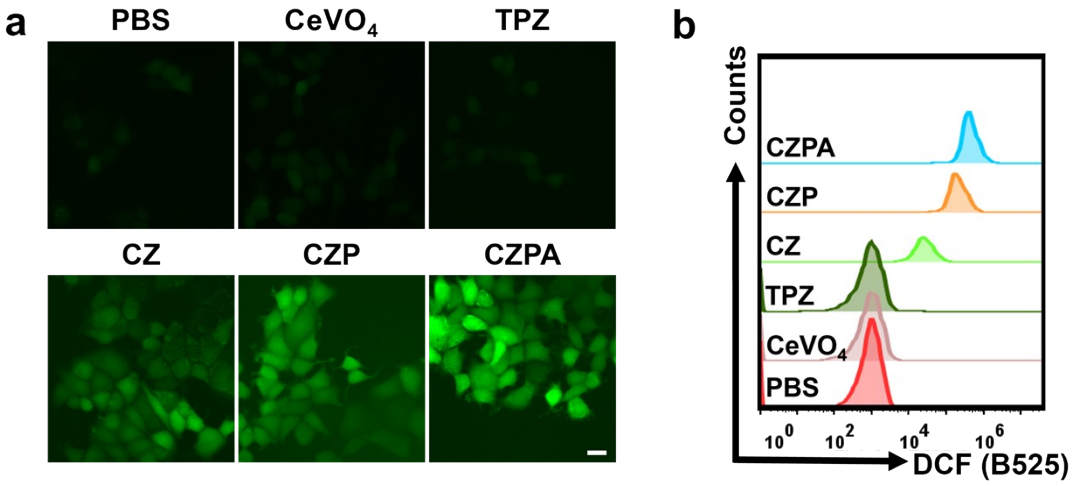

Fig. S24. (a) Fluorescence images results of MCF-7 cells with different treatments. Scale bar: 20 μm. (b) Flow cytometry analyses of MCF-7 cells incubated with different nanoparticles.

The fluorescent chemical 2',7'-dichlorofluorescein (DCF) can be produced by oxidation of this molecule by ROS.[15,34] In the control cells and those treated with $CeVO_4$, weak DCF fluorescence was observed, which could be explained by the ROS that the cells themselves produce.[35,36] Additionally, there was little fluorescence in the TPZ-treated cells because the hypoxia-activatable drug is not harmful in the nonhypoxic environment. The increased fluorescence signals seen in the cells treated with CZ, CZP, or CZPA, as compared to the controls, could potentially be linked to the rise in ROS production. This increase in ROS is likely a result of oxygen consumption facilitated by the $CeVO_4$-induced CcO-like reaction, as well as the ROS generated by TPZ in response to these changes.

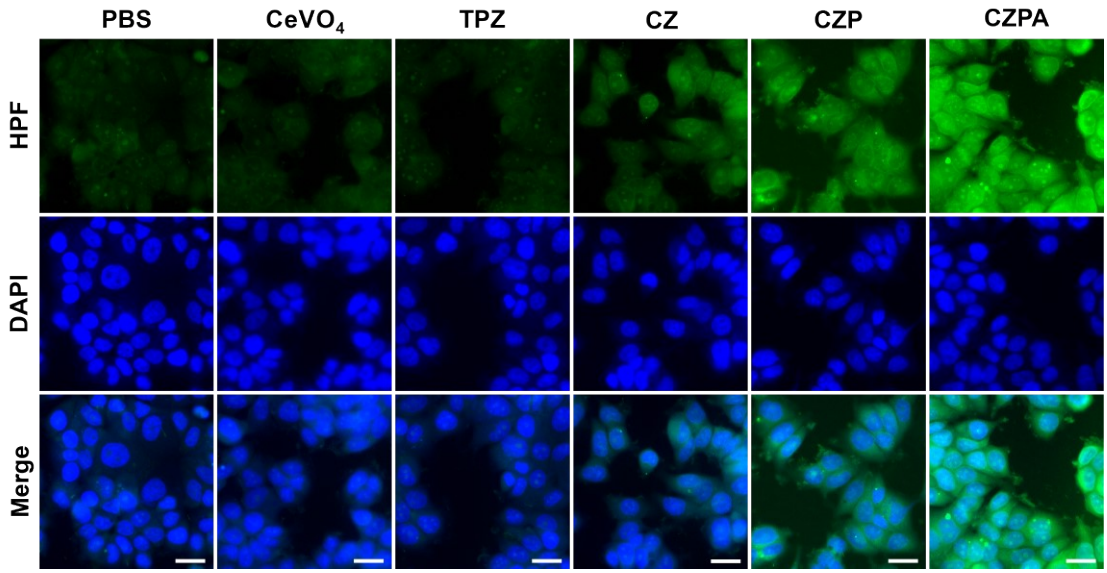

Fig. S25. Fluorescence images of ·OH generation in MCF-7 cells using HPF probe. Scale bar: 10 μm.

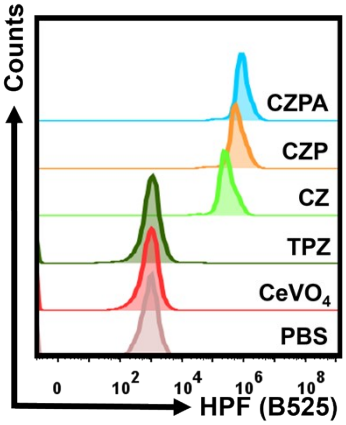

Fig. S26. Flow cytometry analyses of MCF-7 cells exposed with various nanoparticles.

Compared with PBS group, $CeVO_4$ group and TPZ group, the fluorescence intensity and flow cytometric analysis of CZ group was significantly enhanced due to TPZ can be activated with $CeVO_4$ to produce OH. Moreover, the CZPA group showed further enhanced fluorescence as a result of the increase in internalization mediated by the Apt, which indicated intracellular •OH concentration increasing.

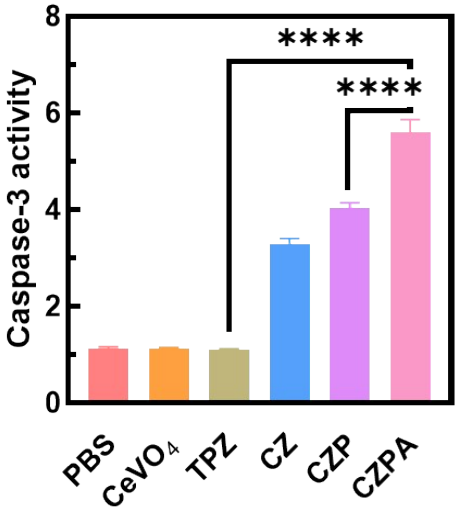

Fig. S27. Caspase-3 activity with the use of an activity detection kit analysis. Mean ± SD (n = 3). ****P < 0.0001.

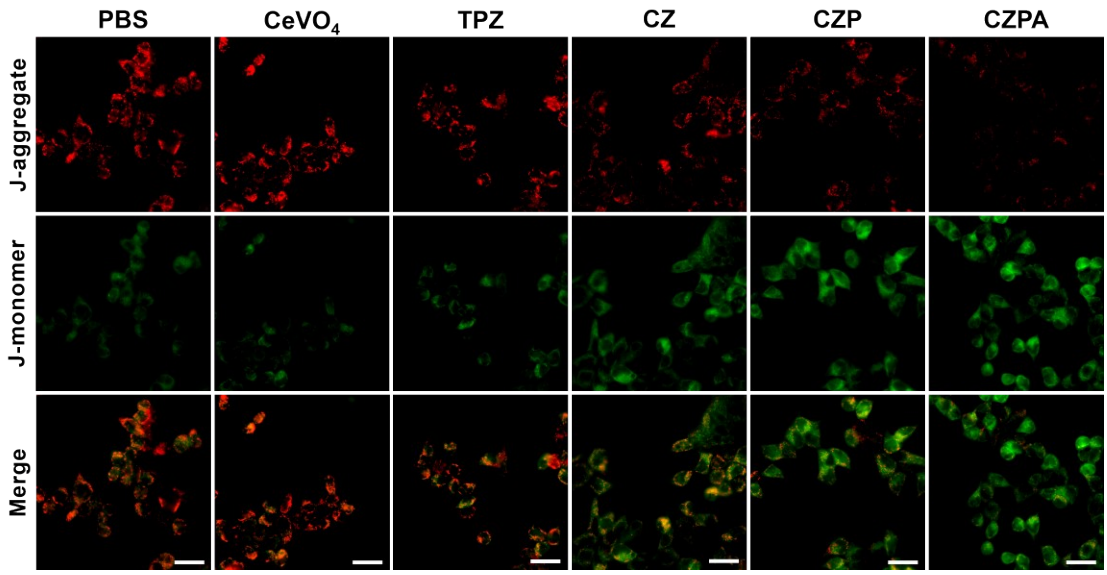

Fig. S28. Fluorescence images of MMP of MCF-7 cells following various treatments. Scale bar: 20 μm.

JC-1 aggregates to produce unique granular red fluorescence spots in healthy mitochondria. Mitochondrial damage is indicated by the elevated green fluorescence signal. The green fluorescence signal increases when mitochondria are injured and the membrane potential drops, allowing JC-1 to scatter in the cytoplasmic matrix in monomeric states.[37] The data gathered in the red channel, which was identical to the PBS group, showed that the $CeVO_4$ incubation did not interfere with mitochondria. On the contrary, the cells treated with CZ、CZP and CZPA stimulated by hypoxia to produce ROS, the green fluorescence signal substantially increased whereas the red fluorescence signal was noticeably suppressed.

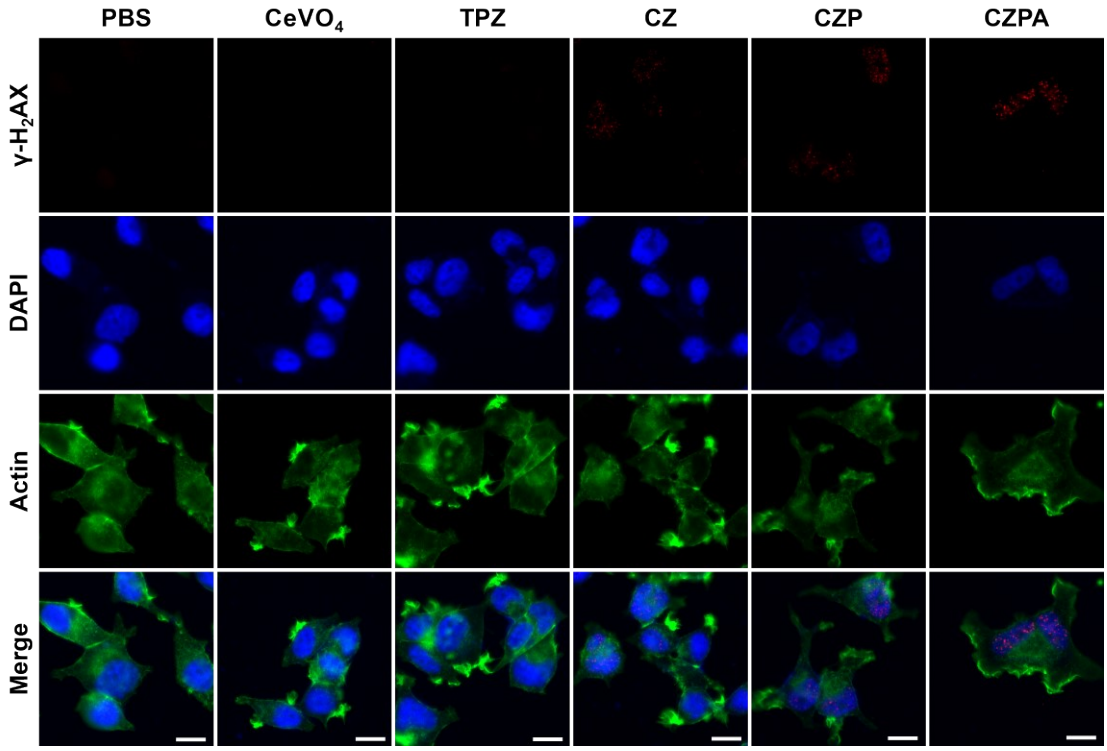

Fig. S29. γ-H_2AX immunofluorescence staining images in MCF-7 cells with different nanoparticles. Scale bar: 20 μm.

γ-H_2AX which is a phosphorylated form of H_2AX and serves as a marker for DNA damage. γ-H_2AX is labeled by antigen−antibody reaction. If DNA damage has occurred, red fluorescence can be observed, with the fluorescence intensity correlating with the degree of DNA damage.[38, 39] MCF-7 cells were exposed to a variety of treatments in order to look into the possible mechanism by which CZPA NC causes tumor cell death. The red fluorescence intensity of $CeVO_4$ NPs and TPZ treated group were similar to that of control and did not show significant DNA damage effects to MCF-7 cells, which indicated that TPZ did not exhibit obvious cytotoxicity under normoxic conditions. Clearly, in comparison to the other groups, the CZPA group showed considerably more severe DNA damage.

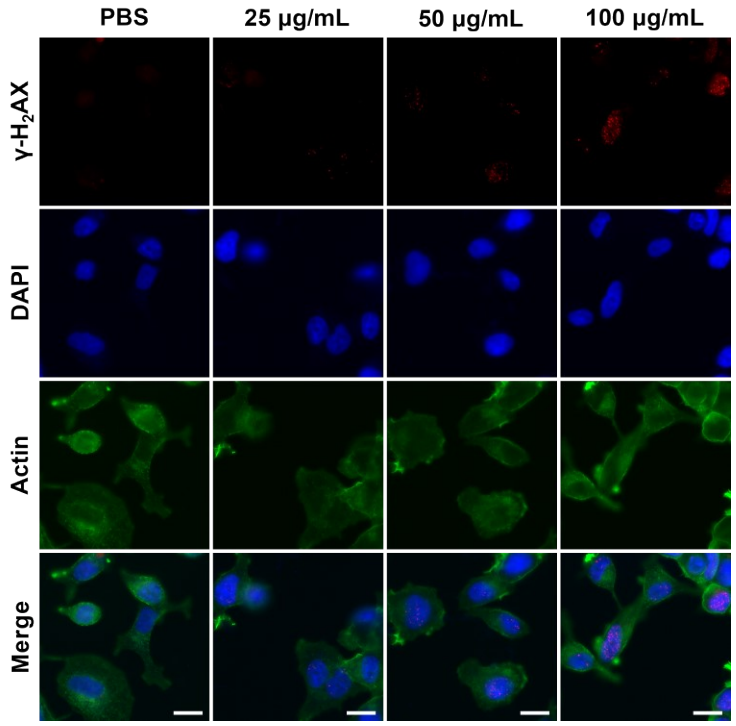

Fig. S30. γ-H_2AX immunofluorescence staining images of MCF-7 cells treated with CZPA NC at various concentrations. Scale bar: 20 μm.

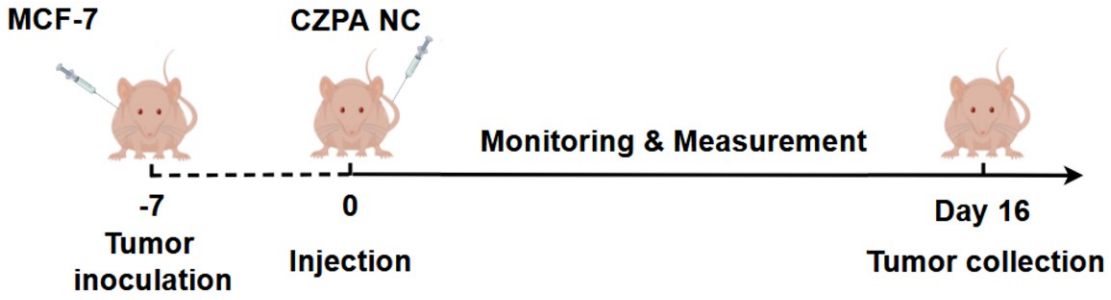

Fig. S31. Treatment protocol design for MCF-7 model tumor-bearing mice.

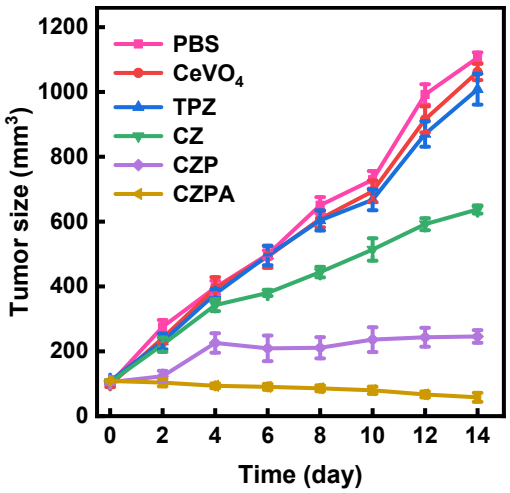

Fig. S32. Tumor growth curves after different treatments.

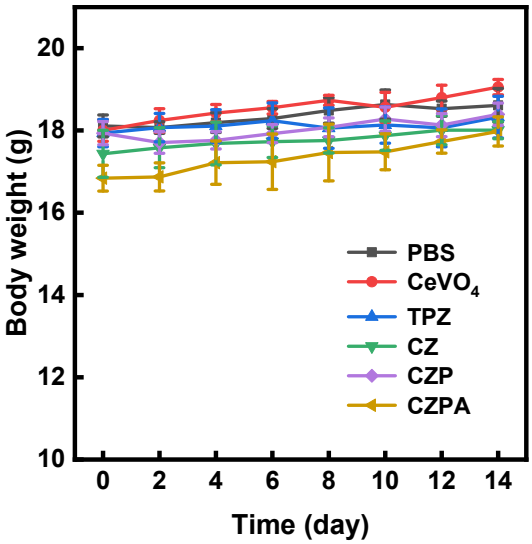

Fig. S33. Body weight changes of the mice after different treatments.

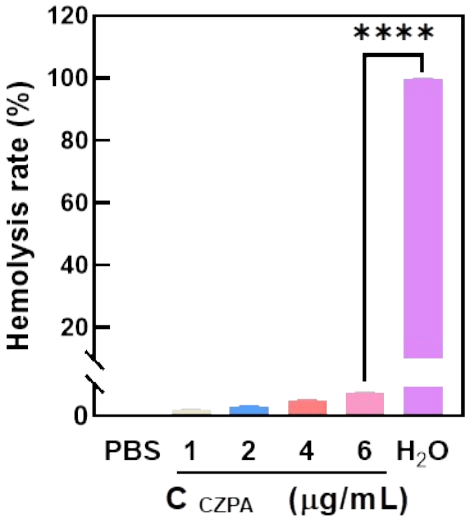

Fig. S34. The corresponding hemolysis rate after treatment with different concentrations of CZPA. Mean ± SD (n = 3). ****P < 0.0001.

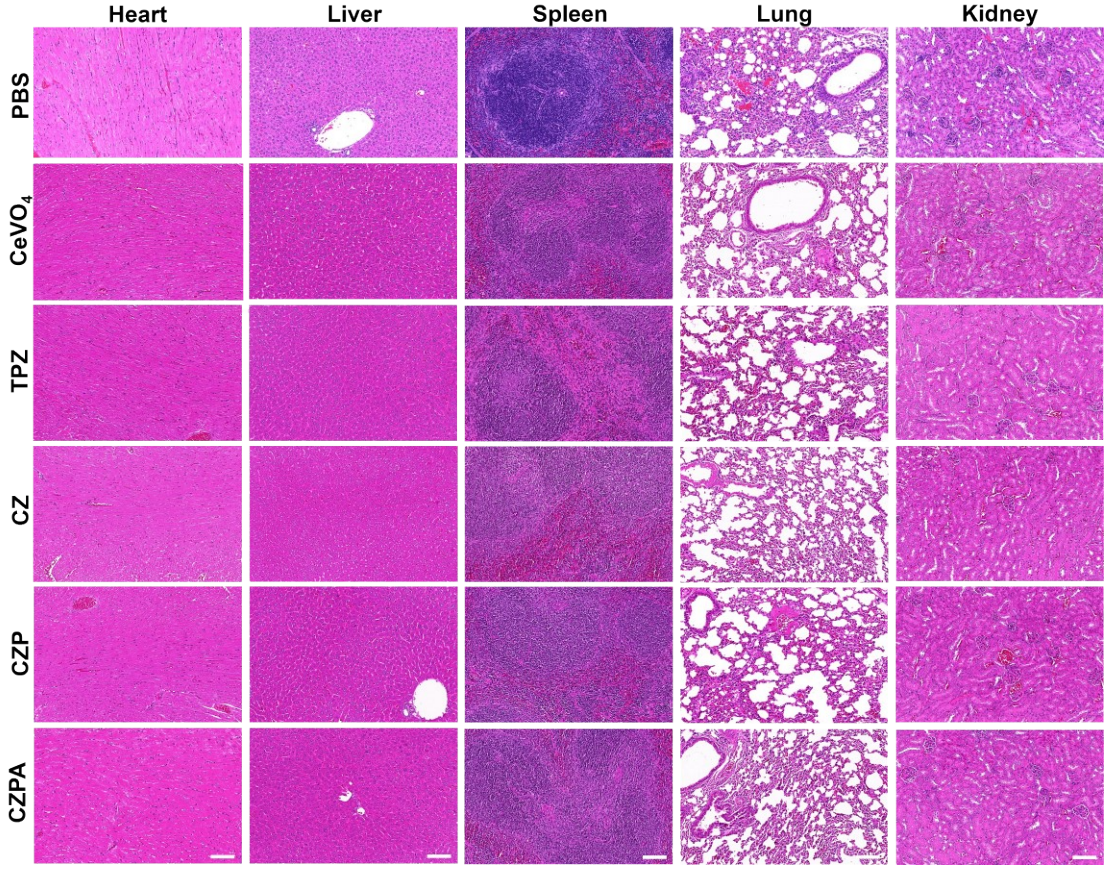

Fig. S35. Biosafety was evaluated by H&E staining of heart, liver, spleen, lung, and kidney. Scale bar: 100 μm.

Notes and references

1 Y. Zhang, Q. Wang, G. Chen and P. Shi, *Inorg. Chem.*, 2019, **58**, 6593-6596.

2 C. Creutz and N. Sutin, *PNAS*, 1973, **70**, 1701-1703.

3 A. V. Peskin and C. C. Winterbourn, *Clin. Chim. Acta*, 2000, **293**, 157-166.

4 M. Zhou, Z. Diwu, N. Panchuk-Voloshina and R. P. Haugland, *Anal. Biochem.*, 1997, **253**, 162-168.

5 P. Karam and L. I. Halaoui, *Anal. Chem.*, 2008, **80**, 5441-5448.

6 E. G. Heckert, A. S. Karakoti, S. Seal and W. T. Self, *Biomaterials*, 2008, **29**, 2705-2709.

7 X. Chen, X. Tian, I. Shin and J. Yoon, *Chem. Soc. Rev.*, 2011, **40**, 4783-4804.

8 M. Chen, Z. H. Wang, J. X. Shu, X. H. Jiang, W. Wang, Z. H. Shi and Y. W. Lin, *Inorg. Chem.*, 2017, **56**, 9400-9403.

9 N. Singh and G. Mugesh, *Angew. Chem. Int. Ed.*, 2019, **58**, 7797-7801.

10 K. Zhang, Y. Zhang, X. Meng, H. Lu, H. Chang, H. Dong and X. Zhang, *Biomaterials*, 2018, **185**, 301-309.

11 Z. Y. Ma, Y. F. Zhang, X. X. Dai, W. Y. Zhang, M. F. Foda, J. Zhang, Y. L. Zhao and H. Y. Han, *Adv. Mater.*, 2021, **33**, 2104504.

12 Y. Zhang, Q. Jia, F. Nan, J. Wang, K. Liang, J. Li, X. Xue, H. Ren, W. Liu, J. Ge and P. Wang, *Biomaterials*, 2023, **293**, 121953.

13 D. Chen, J. Zhang, Y. Tang, X. Huang, J. Shao, W. Si, J. Ji, Q. Zhang, W. Huang and X. Dong, *J. Mater. Chem. B*, 2018, **6**, 4522-4530.

14 N. Lu, W. Fan, X. Yi, S. Wang, Z. Wang, R. Tian, O. Jacobson, Y. Liu, B. C. Yung, G. Zhang, Z. Teng, K. Yang, M. Zhang, G. Niu, G. Lu and X. Chen, *ACS Nano*, 2018, **12**, 1580-1591.

15 Y. Guo, H.-R. Jia, X. Zhang, X. Zhang, Q. Sun, S.-Z. Wang, J. Zhao and F.-G. Wu, *Small*, 2020, **16**, 2000897.

16 X. L. Ding, M. D. Liu, Q. Cheng, W. H. Guo, M. T. Niu, Q. X. Huang, X. Zeng and X. Z. Zhang, *Biomaterials*, 2022, **281**, 121369.

17 J. J. Liu, F. Hu, M. Wu, L. L. Tian, F. Gong, X. Y. Zhong, M. C. Chen, Z. Liu and B. Liu, *Adv. Mater.*, 2021, **33**, 2007888.

18 X. He, Y. Dong, P. He, C. Liu and W. Ren, *J. Anal. Test.*, 2024, **8**, 270-277.

19 Y. Ji, S. Qu, G. Shi, L. Fan, J. Qian, Z. Sun, F. Lu and X. Han, *ACS Nano*, 2024, **18**, 31421-31434.

20 Q. Zheng, H. H. Liu, H. Zhang, Y. B. Han, J. X. Yuan, T. T. Wang, Y. F. Gao and Z. Li, *Adv. Sci.*, 2023, **10**.

21 M. R. Dreher, W. Liu, C. R. Michelich, M. W. Dewhirst, F. Yuan and A. Chilkoti, *JNCI: Journal of the National Cancer Institute*, 2006, **98**, 335-344.

22 F. Alexis, E. Pridgen, L. K. Molnar and O. C. Farokhzad, *Mol. Pharmaceutics*, 2008, **5**, 505-515.

23 Z. Zheng, D. Peng, M. Li, X. Lu, S. Gong, Y. Yuan, E. K. Silli, J. Tang, Q. Zhao, H. Xu, Y.

Lan, C. Tan and Y. Wang, *J. Drug Delivery Sci. Technol.*, 2023, **87**, 104872.

24 A. Yan, X. Q. Chen, J. He, Y. F. Ge, Q. Liu, D. Men, K. Xu and D. Li, *Angewandte Chemie-International Edition*, 2023, **62**.

25 F. Luo, C.-J. Jia, W. Song, L.-P. You and C.-H. Yan, *Crystal Growth & Design*, 2005, **5**, 137-142.

26 N. Singh and G. Mugesh, *Angew. Chem. Int. Ed.*, 2019, **58**, 7797-7801.

27 J. Z. He, J. H. Zhao, Z. Run, M. J. Sun and H. Pang, *Chemistry-an Asian Journal*, 2015, **10**, 338-343.

28 J. Hou, H. Huang, Z. Han and H. Pan, *RSC Adv.*, 2016, **6**, 14552-14558.

29 U. Opara Krašovec, B. Orel, A. Šurca, N. Bukovec and R. Reisfeld, *Solid State Ionics*, 1999, **118**, 195-214.

30 D. L. Mendez, S. E. Babbitt, J. D. King, J. D'Alessandro, M. B. Watson, R. E. Blankenship, L. M. Mirica and R. G. Kranz, *PNAS*, 2017, **114**, 2235-2240.

31 E. Margoliash and N. Frohwirt, *Biochem. J*, 1959, **71**, 570-572.

32 J. Mu, L. Zhang, M. Zhao and Y. Wang, *ACS Appl. Mater. Interfaces*, 2014, **6**, 7090-7098.

33 L. Ge, C. Qiao, Y. Tang, X. Zhang and X. Jiang, *Nano Lett.*, 2021, **21**, 3218-3224.

34 W. Li, L. Sun, X. Zheng, F. Li, W. Zhang, T. Li, Y. Guo and D. J. A. C. Tang, *Anal. Chem.*, 2023, **95**, 9654-9662.

35 S. Zhang, Y. Yang, Y. Zhang, J. Zhang, L. Li, C. Liu and Q. Wu, *J. Anal. Test.*, 2023, **7**, 227-236.

36 J. Chen, H. Liu, W. Xie, M. Gu, G. Mao and S. Yang, *J. Anal. Test.*, 2023, **7**, 304-324.

37 H. Zhang, C. Shi, F. Han, L. Cai, H. Ma, S. Long, W. Sun, J. Du, J. Fan, X. Chen and X. Peng, *Biomaterials*, 2023, **302**, 122365.

38 Y. Lu, D. Jia, X. Ma, M. Liang, S. Hou, W. Qiu, Y. Gao, P. Xue, Y. Kang and Z. Xu, *ACS Appl. Mater. Interfaces*, 2021, **13**, 8940-8951.

39 M. Liang, Y. Gao, W. Qiu, M. Ye, J. Hu, J. Xu, P. Xue, Y. Kang and Z. Xu, *ACS Appl. Mater. Interfaces*, 2021, **13**, 37680-37692.